Journal of Fundamental and Applied Research **Vol. 5**, Issue 2 (2025) **20250008**

Received: 02 May 2025 / Accepted: 25 June 2025
Published online: 27 June 2025
© 2025 The Author(s)

Two-gap model analysis of the London penetration depth and lower critical field in $SmFeAsO_{1-x}F_x$ and LiFeAs superconductors

Orifjon Ganiev[1, 2, *] and Zakhriddin Rakhmonov[3]

[1] *Institute of Nuclear Physics, AS RUz, 100214 Tashkent, Uzbekistan*
[2] *National University of Uzbekistan, 100174 Tashkent, Uzbekistan*
[3] *Engineering Physics Institute, Samarkand State University, 140104 Samarkand, Uzbekistan*

Abstract. We present a theoretical investigation of the superfluid response in iron-based superconductors (FeSCs) using a self-consistent two-gap model. This approach is motivated by the multiband electronic structure intrinsic to these materials, which leads to the formation of multiple distinct superconducting energy gaps. Within this framework, we calculate the temperature dependence of key thermodynamic and electromagnetic properties, including the superfluid density (ρ_s), the London penetration depth (λ_L), and the lower critical magnetic field (H_{c1}). We perform a comparative analysis against a standard single-gap Bardeen-Cooper-Schrieffer (BCS) model and against experimental data for representative FeSC compounds, including $SmFeAsO_{1-x}F_x$ and LiFeAs. The results demonstrate that the two-gap model provides a significantly improved, and often quantitative, description of the experimental data over the entire temperature range below the critical temperature, T_c. In contrast, the single-gap BCS model fails to capture crucial features, such as the low-temperature saturation of $\rho_s(T)$ and $\lambda_L(T)$. The theoretical predictions are in good quantitative agreement with experimental data, validating the two-band model and emphasizing the essential role of multiband physics in governing the superconducting state of FeSCs.

Keywords: Iron-based superconductors, two-gap model, superfluid density, London penetration depth, lower critical field

I. INTRODUCTION

The discovery of iron-based superconductors (FeSCs) in 2008 [1] opened a new frontier in condensed matter physics, offering a fresh platform to study unconventional superconductivity. These materials exhibit a rich phase diagram with a complex interplay between superconductivity, magnetism, and structural transitions [2]. Unlike conventional superconductors, which are well-described by the Bardeen-Cooper-Schrieffer (BCS) theory of phonon-mediated electron pairing [3], FeSCs possess a complex, multi-orbital electronic structure. This leads to multiple bands crossing the Fermi level, which is a key ingredient for the emergence of multiple superconducting gaps [4, 5].

Understanding the superconducting state requires probing its fundamental properties. Three crucial parameters are the superfluid density (ρ_s), the London penetration depth (λ_L), and the lower critical field (H_{c1}). The superfluid density reflects the number density of superconducting charge carriers (Cooper pairs) and the rigidity of the superconducting condensate [6]. The penetration depth, λ_L, is the characteristic length scale over which an external magnetic field is screened and is inversely related to the superfluid density, $\lambda_L \propto 1/\sqrt{\rho_s}$. The lower critical field, H_{c1}, marks the energetic threshold for magnetic flux penetration into a type-II superconductor.

Experimental measurements on FeSCs reveal a diverse range of behaviors for these quantities. Techniques such as muon spin rotation (μSR) [7, 8], microwave cavity perturbation, and measurements of H_{c1} [9, 10] have been pivotal. While some FeSCs show a low-temperature saturation of $\rho_s(T)$, characteristic of a fully gapped (nodeless) superconductor, others exhibit power-law dependencies that suggest the presence of nodes in the superconducting gap [11]. A key recurring feature in many FeSCs is the evidence for two distinct superconducting gaps [12–14]. This "two-gap" behavior manifests as changes in the temperature dependence of quantities like $\rho_s(T)$ and is a direct consequence of the multiband electronic structure.

* Corresponding author: oganiev@yahoo.com

To describe this phenomenology, simple extensions of the BCS theory, such as the phenomenological α-model which sums two independent BCS-like contributions, have been employed [15, 16]. However, such models are not fully self-consistent as they ignore the crucial role of interband scattering, which is necessary to explain the existence of a single, sharp superconducting transition temperature T_c. A more rigorous approach is the self-consistent two-gap model, originally proposed by Suhl, Matthias, and Walker [17] and Moskalenko [18].

In this paper, we employ a self-consistent two-band model to analyze the superfluid response of FeSCs. We solve the coupled gap equations numerically to obtain the temperature dependence of the two energy gaps, $\Delta_1(T)$ and $\Delta_2(T)$. From these, we calculate $\rho_s(T)$, $\lambda_L(T)$, and $H_{c1}(T)$ and compare our results directly with experimental data for the well-studied compounds $SmFeAsO_{1-x}F_x$ and LiFeAs. We demonstrate that this model, which explicitly includes both intraband and interband pairing interactions, provides excellent quantitative agreement with the data and explains the observed deviations from single-gap BCS theory, thereby highlighting the indispensable role of multiband physics in these materials.

II. THEORETICAL FRAMEWORK

We model the multigap superconductivity in FeSCs using a self-consistent two-band approach for isotropic s-wave gaps. This model builds upon the original works of Suhl et al. [17] and Moskalenko [18] and was later refined for FeSCs by others [13, 19, 20].

A. Coupled Gap Equations

The central elements of the model are the two superconducting gaps, Δ_1 and Δ_2, associated with two distinct electronic bands. Their temperature dependencies are determined by solving a set of coupled integral equations:

$$\begin{aligned}\Delta_1(T) = \int_0^{\hbar\omega_D} d\varepsilon \left[V_{11}N_1(0)\frac{\Delta_1(T)}{\sqrt{\varepsilon^2+\Delta_1(T)^2}}\tanh\left(\frac{\sqrt{\varepsilon^2+\Delta_1(T)^2}}{2k_BT}\right)\right.\\ \left. +V_{12}N_2(0)\frac{\Delta_2(T)}{\sqrt{\varepsilon^2+\Delta_2(T)^2}}\tanh\left(\frac{\sqrt{\varepsilon^2+\Delta_2(T)^2}}{2k_BT}\right)\right]\\ \Delta_2(T) = \int_0^{\hbar\omega_D} d\varepsilon \left[V_{21}N_1(0)\frac{\Delta_1(T)}{\sqrt{\varepsilon^2+\Delta_1(T)^2}}\tanh\left(\frac{\sqrt{\varepsilon^2+\Delta_1(T)^2}}{2k_BT}\right)\right.\\ \left. +V_{22}N_2(0)\frac{\Delta_2(T)}{\sqrt{\varepsilon^2+\Delta_2(T)^2}}\tanh\left(\frac{\sqrt{\varepsilon^2+\Delta_2(T)^2}}{2k_BT}\right)\right]\end{aligned} \tag{1}$$

Here, $N_j(0)$ is the single-spin density of states at the Fermi level for band j, V_{jj} are the intraband pairing potentials, and V_{ij} ($i \neq j$) are the interband pairing potentials that couple the two bands. For simplicity, we assume a common Debye cutoff frequency, ω_D. The crucial feature is the interband coupling (V_{12}, V_{21}), which scatters Cooper pairs between bands and is responsible for establishing a single critical temperature, T_c, for the entire system.

By defining the dimensionless coupling constants $\lambda_{ij} = N_j(0)V_{ij}$, Eq. (1) can be written more compactly as:

$$\begin{aligned}\Delta_1 &= \lambda_{11}\Delta_1 I(\Delta_1, T) + \lambda_{12}\Delta_2 I(\Delta_2, T)\\ \Delta_2 &= \lambda_{21}\Delta_1 I(\Delta_1, T) + \lambda_{22}\Delta_2 I(\Delta_2, T)\end{aligned} \tag{2}$$

where $I(\Delta, T) = \int_0^{\hbar\omega_D} d\varepsilon (1/\sqrt{\varepsilon^2+\Delta^2})\tanh(\sqrt{\varepsilon^2+\Delta^2}/2k_BT)$. The superconducting transition temperature T_c is determined by the condition that a non-trivial solution to these linearized equations exists. This leads to an expression for T_c:

$$T_c = \frac{2\gamma_E\hbar\omega_D}{\pi k_B}e^{-1/\lambda_{\text{eff}}} \tag{3}$$

where $\gamma_E \approx 1.78$ is Euler's constant and λ_{eff} is the largest eigenvalue of the coupling matrix $\lambda = \begin{pmatrix}\lambda_{11} & \lambda_{12}\\ \lambda_{21} & \lambda_{22}\end{pmatrix}$:

$$\lambda_{\text{eff}} = \frac{\lambda_{11}+\lambda_{22}}{2} + \sqrt{\frac{(\lambda_{11}-\lambda_{22})^2}{4} + \lambda_{12}\lambda_{21}}. \tag{4}$$

B. Superfluid Density and Related Quantities

The normalized superfluid density for a single s-wave gap $\Delta(T)$ within BCS theory is given by

$$\frac{\rho_s(T)}{\rho_s(0)} = 1 - \frac{1}{2k_BT}\int_0^\infty \text{sech}^2\left(\frac{\sqrt{\varepsilon^2+\Delta(T)^2}}{2k_BT}\right) d\varepsilon. \tag{5}$$

In our two-band model, the total superfluid density is a weighted sum of the contributions from each band:

$$\frac{\rho_s(T)}{\rho_s(0)} = w_\rho \frac{\rho_{s1}(T)}{\rho_{s1}(0)} + (1-w_\rho)\frac{\rho_{s2}(T)}{\rho_{s2}(0)}, \tag{6}$$

where each term $\rho_{sj}(T)/\rho_{sj}(0)$ is calculated using Eq. (5) with its respective gap $\Delta_j(T)$. The weighting factor w_ρ represents the fractional contribution of the first band to the total superfluid density at $T = 0$.

The London penetration depth $\lambda_L(T)$ is fundamentally linked to the superfluid density:

$$\frac{\lambda_L^2(0)}{\lambda_L^2(T)} = \frac{\rho_s(T)}{\rho_s(0)}, \tag{7}$$

where $\lambda_L(T) = \sqrt{m^*/(\mu_0 e^2 \rho_s(T))}$, with m^* being the effective mass of the charge carriers. This relation allows for a direct comparison between our calculated superfluid density and experimental measurements of the penetration depth.

Finally, the lower critical field $H_{c1}(T)$ can be calculated within the Ginzburg-Landau theory. For a type-II superconductor with a large Ginzburg-Landau parameter $\kappa = \lambda_L/\xi \gg 1$, as is typical for FeSCs, H_{c1} is given by:

$$H_{c1}(T) = \frac{\Phi_0}{4\pi\mu_0\lambda_L^2(T)}\left[\ln\kappa(T) + 0.5\right], \tag{8}$$

where $\Phi_0 = h/2e$ is the magnetic flux quantum and ξ is the superconducting coherence length. The dominant temperature dependence in Eq. (8) comes from $\lambda_L^2(T)$, making $H_{c1}(T)$ a sensitive probe of the superfluid density and the underlying gap structure.

III. RESULTS AND COMPARISON WITH EXPERIMENT

We apply the theoretical framework described in Sec. II to two families of iron-based superconductors, $SmFeAsO_{1-x}F_x$ and LiFeAs, which are well-known to exhibit multigap features. The procedure involves solving Eq. (2) for $\Delta_j(T)$ using a set of coupling parameters λ_{ij} chosen to reproduce the experimental T_c and match the observed behavior of superfluid density.

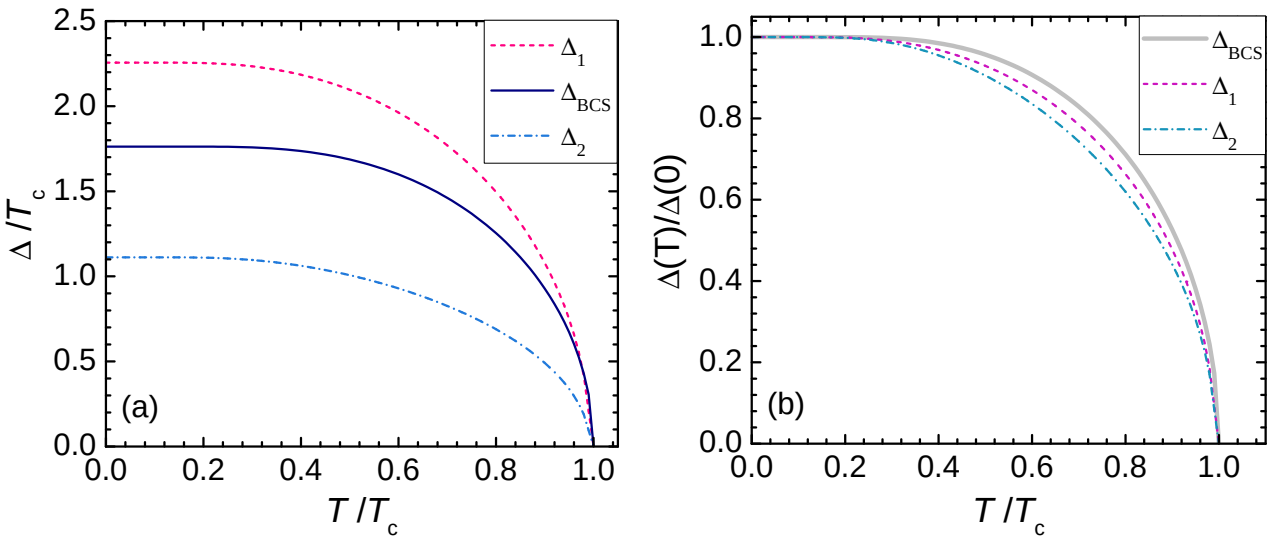


Figure 1. Calculated temperature dependence of the superconducting gaps for $SmFeAsO_{0.8}F_{0.2}$ ($T_c = 44$ K). (a) The two gaps, $\Delta_1(T)$ and $\Delta_2(T)$, vanish at the same T_c. The larger gap Δ_1 stems from stronger intraband coupling λ_{11}. (b) The same gaps normalized to their zero-temperature values, compared with the standard BCS temperature dependence (dashed line).

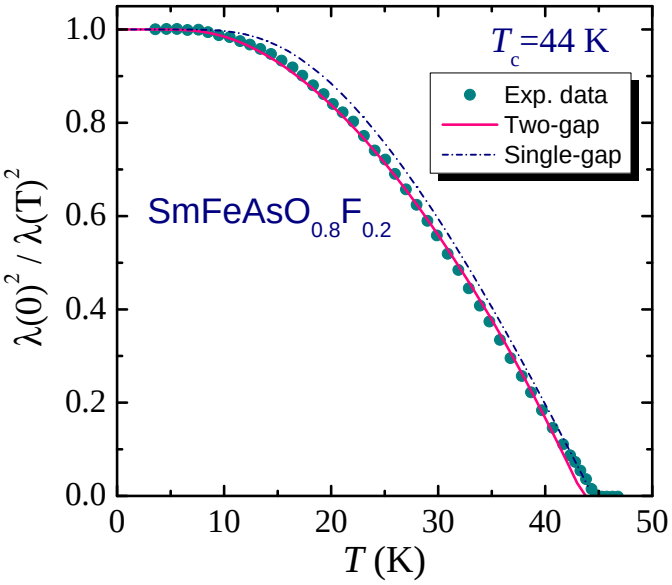


Figure 2. Comparison of theoretical predictions for the normalized superfluid density of $SmFeAsO_{0.8}F_{0.2}$ with experimental data from Ref. [21]. The two-gap model (solid line) accurately describes the data, whereas the single-gap BCS model (dashed line) fails, particularly at low temperatures.

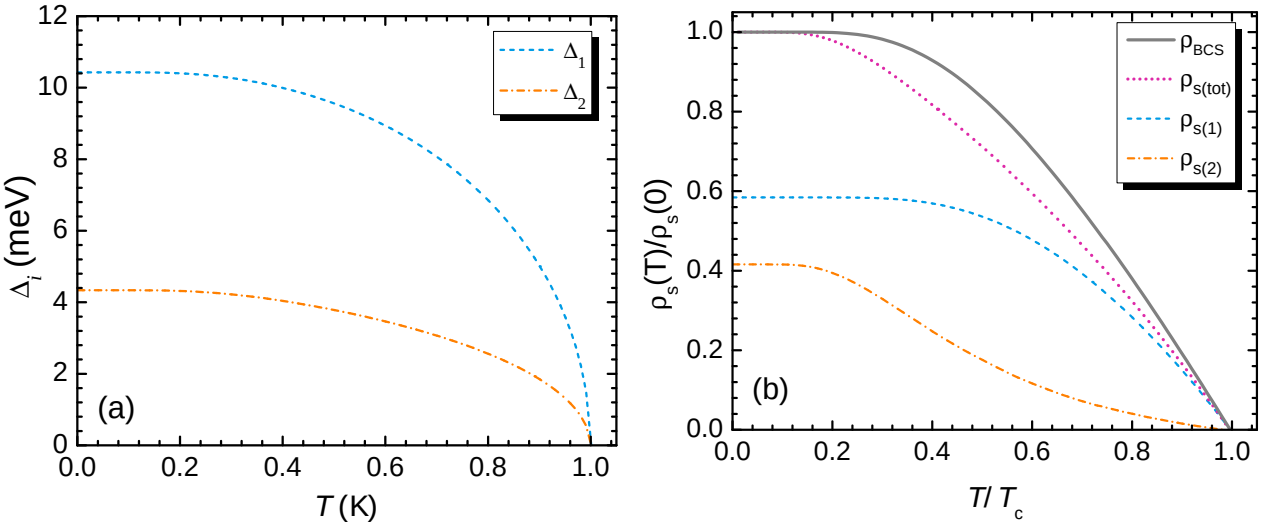


Figure 3. Theoretical analysis for $SmFeAsO_{0.9}F_{0.1}$ ($T_c = 53$ K). (a) Temperature dependence of the two gaps, $\Delta_1(T)$ and $\Delta_2(T)$. (b) Total normalized superfluid density and its decomposition into contributions from band 1 (ρ_{s1}) and band 2 (ρ_{s2}).

We first model the compound $SmFeAsO_{0.8}F_{0.2}$. Based on experimental reports, we use a set of parameters consistent with the observed properties: $T_c = 44$ K, band weight $w_\rho = 0.67$, and coupling constants $\lambda_{11} = 1.23$, $\lambda_{12} = \lambda_{21} = 0.48$, and $\lambda_{22} = 0.38$.

The resulting temperature dependence of the two gaps is shown in Fig. 1. At $T = 0$, the model yields two distinct gap values, with the larger gap Δ_1 originating from the band with the stronger intraband coupling (λ_{11}). Both gaps vanish at the same critical temperature $T_c = 44$ K due to the finite interband coupling (λ_{12}).

From these gaps, we calculate the total normalized superfluid density $\rho_s(T)/\rho_s(0)$ using Eq. (6). Figure 2 shows this result and compares it with both the single-gap BCS prediction and experimental data obtained from penetration depth measurements [21]. The failure of the single-gap BCS model is striking; it predicts a much more rapid decrease of $\rho_s(T)$ with temperature and completely misses the characteristic flattening observed in the experiment at low temperatures. In contrast, our two-gap calculation shows excellent agreement with the experimental data across the entire temperature range. The low-temperature saturation is a hallmark of a fully gapped superconductor, which our two-band model naturally reproduces.

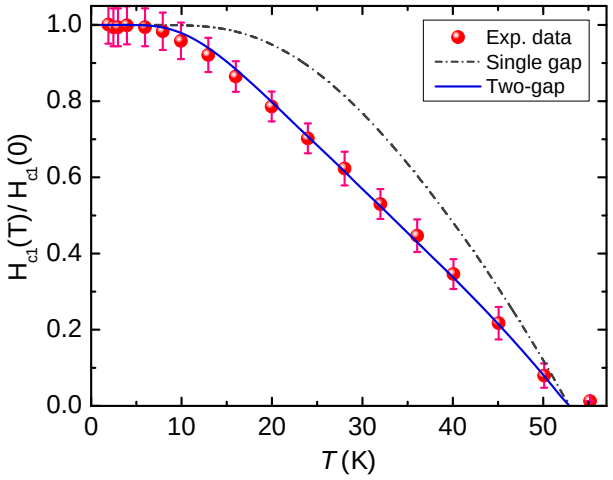


Figure 4. Comparison of theoretical predictions for the normalized lower critical field $H_{c1}(T)/H_{c1}(0)$ of $SmFeAsO_{0.9}F_{0.1}$ with experimental data from Ref. [22]. The two-gap model provides an excellent description of the data, unlike the single-gap BCS model.

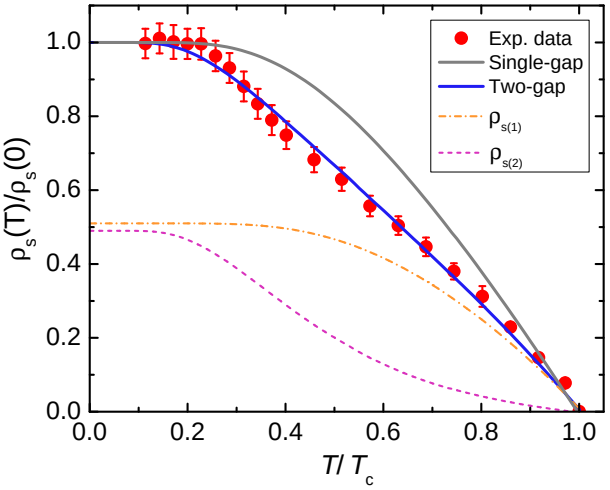


Figure 5. Normalized superfluid density $\rho_s(T)/\rho_s(0)$ for LiFeAs. The experimental data (symbols) from Ref. [14] are well-described by the two-gap model calculation (solid blue line) and its individual band contributions (ρ_{s1}, ρ_{s2}). The single-gap BCS prediction (gray line) clearly fails to capture the low-temperature saturation.

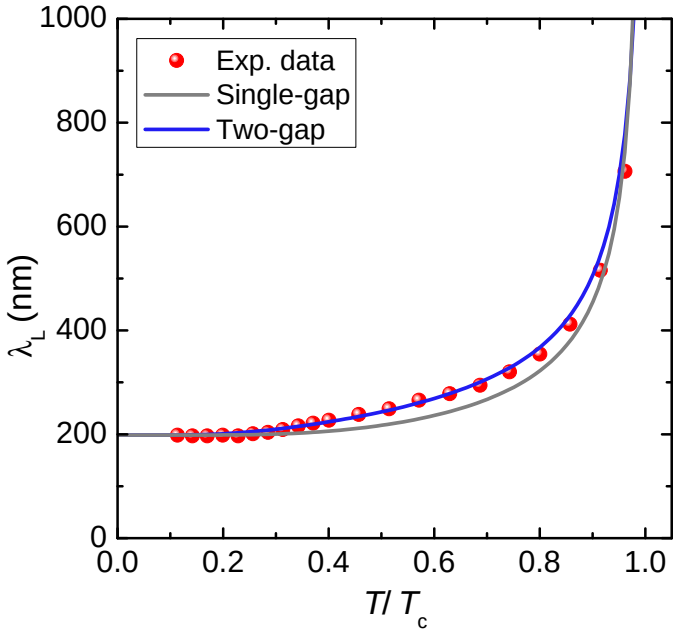


Figure 6. Temperature dependence of the London penetration depth $\lambda_L(T)$ for LiFeAs. The two-gap model calculation (blue line) is in excellent agreement with the experimental data from Ref. [14], accurately capturing the very weak temperature dependence at low T. The single-gap BCS model (gray line) predicts a much steeper rise.

We further extend our analysis to the related compound $SmFeAsO_{0.9}F_{0.1}$ ($T_c = 53$ K). The parameters for this system are chosen as $m^* = 3m_e$, $w_\rho = 0.584$, $\lambda_{11} = 1.64$, $\lambda_{12} = \lambda_{21} = 0.52$, and $\lambda_{22} = 0.4$. This parameter set reflects stronger overall coupling, consistent with the higher T_c.

Figure 3(a) shows the calculated gaps for this material. The larger zero-temperature gap splitting is a direct consequence of the greater disparity in the intraband coupling strengths ($\lambda_{11} \gg \lambda_{22}$). Figure 3(b) displays the total superfluid density and its decomposition into the individual band contributions. The component from band 1, associated with the larger gap Δ_1, exhibits a very flat, BCS-like behavior. In contrast, the component from band 2, with the smaller gap Δ_2, shows a more pronounced decrease at low temperatures. The total superfluid density is a non-trivial superposition of these two, resulting in the characteristic

shape observed experimentally.

Finally, we test the model by calculating the lower critical field, $H_{c1}(T)$, using the same set of parameters. Figure 4 compares the normalized $H_{c1}(T)/H_{c1}(0)$ from our two-band model with experimental data from Ref. [22] and the prediction from a single-gap BCS model. Again, the agreement between our two-band model and the experiment is excellent. This successful prediction of a different physical quantity using the same microscopic parameters provides strong validation for our approach and demonstrates that the thermodynamic stability against flux penetration is governed by the same underlying two-gap electronic structure.

To demonstrate the broad applicability of the model, we now turn to LiFeAs, a stoichiometric iron pnictide that is also a known multigap superconductor. We analyze the experimental penetration depth data from Song et al. [14]. The parameters for our calculation are chosen to match the experimental findings for LiFeAs: $T_c = 17.5$ K, $m^* = 2.5m_e$, $w_\rho = 0.65$, $\lambda_{11} = 1.38$, $\lambda_{12} = \lambda_{21} = 0.33$, and $\lambda_{22} = 0.43$.

Figure 5 presents the calculated normalized superfluid density and its comparison with experimental data. As with the Sm-based compounds, the two-gap model perfectly captures the pronounced saturation of $\rho_s(T)$ at low temperatures, while the single-gap BCS theory deviates significantly. Song et al. concluded that a two-gap model was essential to fit their data [14]; our self-consistent calculation provides a strong theoretical underpinning for this conclusion.

This agreement is further illustrated in Fig. 6, which plots the temperature-dependent London penetration depth, $\lambda_L(T)$. The plot provides a physically equivalent but visually distinct confirmation of success of the model. The two-gap model correctly reproduces the quasi-temperature-independent behavior of $\lambda_L(T)$ as $T \to 0$, which is the signature of a nodeless, multigap superconducting state. The failure of the single-band model is again obvious. This excellent agreement between our self-consistent calculations and detailed experimental results for LiFeAs underscores that its superconducting phenomenology is intrinsically tied to its multiband electronic structure.

IV. CONCLUSION

We have conducted a comprehensive theoretical analysis of the superfluid response in iron-based superconductors by utilizing a self-consistent, two-band model for s-wave superconductivity. By explicitly incorporating two distinct superconducting gaps (Δ_1, Δ_2) and the crucial interband coupling between them, we have calculated the temperature dependence of the superfluid density (ρ_s), London penetration depth (λ_L), and lower critical field (H_{c1}).

Our comparative analysis demonstrates unequivocally that the single-gap BCS model is insufficient to describe the experimental observations in representative FeSCs like $SmFeAsO_{1-x}F_x$ and LiFeAs. Specifically, it fails to reproduce the saturation of ρ_s and λ_L at low temperatures, a key experimental signature of these fully gapped systems.

In stark contrast, the self-consistent two-band model provides an excellent, and in many cases quantitative, description of the experimental data for $\rho_s(T)$, $\lambda_L(T)$, and $H_{c1}(T)$ over the entire temperature range below T_c. The success of the model stems from its ability to capture the non-trivial superposition of contributions from two different electronic bands, each with a unique gap and temperature evolution, but synchronized by interband scattering to produce a single transition temperature. The ability to describe multiple, distinct physical properties using a single, physically-motivated set of microscopic coupling parameters provides powerful validation for the theoretical framework.

The results presented here provide a robust theoretical basis for interpreting experimental findings in FeSCs, highlighting the distinct signatures of multigap superconductivity in their superfluid response. They confirm that the multiband electronic structure is not merely a detail but a fundamental aspect that governs the thermodynamic and electromagnetic properties of these complex materials.

ACKNOWLEDGEMENTS

The work is financed by the state budget of the Republic of Uzbekistan.

REFERENCES

[1] Y. Kamihara, T. Watanabe, M. Hirano, and H. Hosono, J. Am. Chem. Soc. **130**, 3296 (2008).
[2] G. R. Stewart, Rev. Mod. Phys. **83**, 1589 (2011).
[3] J. Bardeen, L. N. Cooper, and J. R. Schrieffer, Phys. Rev. **108**, 1175 (1957).

[4] P. J. Hirschfeld, M. M. Korshunov, and I. I. Mazin, Rep. Prog. Phys. **74**, 124508 (2011).
[5] R. Prozorov and V. G. Kogan, Rep. Prog. Phys. **74**, 124505 (2011).
[6] M. Tinkham, *Introduction to Superconductivity*, 2nd ed. (Courier Corporation, 1996).
[7] A. Amato, R. Khasanov, H. Luetkens, and H.-H. Klauss, Physica C **469**, 606 (2009).
[8] R. Khasanov, M. Bendele, A. Amato, K. Conder, H. Keller, H.-H. Klauss, H. Luetkens, and E. Pomjakushina, Phys. Rev. Lett. **104**, 087004 (2010).
[9] C. Ren, Z. Wang, H. Luo, H. Yang, L. Shan, and H. Wen, Physica C **469**, 599 (2009).
[10] M. Abdel-Hafiez, P. J. Pereira, S. A. Kuzmichev, T. E. Kuzmicheva, V. M. Pudalov, L. Harnagea, A. A. Kordyuk, A. V. Silhanek, V. V. Moshchalkov, B. Shen, H.-H. Wen, A. N. Vasiliev, and X.-J. Chen, Phys. Rev. B **90**, 054524 (2014).
[11] K. Hashimoto, T. Shibauchi, S. Kasahara, K. Ikada, S. Tonegawa, and Y. Matsuda, Phys. Rev. Lett. **102**, 027002 (2009).
[12] H. Ding, P. Richard, K. Nakayama, K. Sugawara, T. Arakane, Y. Sekiba, A. Takayama, S. Souma, T. Sato, and T. Takahashi, EPL **83**, 47001 (2008).
[13] V. G. Kogan, C. Martin, and R. Prozorov, Phys. Rev. B **80**, 014507 (2009).
[14] Y. J. Song, J. S. Ghim, J. H. Yoon, K. J. Lee, M. H. Jung, H.-S. Ji, J. H. Shim, Y. Bang, and Y. S. Kwon, Europhys. Lett. **94**, 57008 (2011).
[15] A. Carrington and F. Manzano, Physica C **385**, 205 (2003).
[16] H. Padamsee, J. E. Neighbor, and C. A. Shiffman, J. Low. Temp. Phys. **12**, 387 (1973).
[17] H. Suhl, B. T. Matthias, and L. R. Walker, Phys. Rev. Lett. **3**, 552 (1959).
[18] V. A. Moskalenko, Phys. Met. Metallogr. **8**, 25 (1959).
[19] A. Bussmann-Holder, R. Micnas, and A. R. Bishop, Eur. Phys. J. B **37**, 345 (2004).
[20] R. M. Fernandes and J. Schmalian, Phys. Rev. B **82**, 014521 (2010).
[21] A. Carrington, C. R. Phys. **12**, 502 (2011).
[22] Z.-S. Wang, *The superconducting properties research of iron based-122 by transport and scanning micro-squid measurements*, Ph.D. thesis, Université de Grenoble; University of Chinese academy of sciences (2012).